



**HAL**  
open science

# Real-Time Monitoring of Aurora kinase A Activation using Conformational FRET Biosensors in Live Cells

Giulia Bertolin, Gilles Le Marchand, Marc Tramier

► **To cite this version:**

Giulia Bertolin, Gilles Le Marchand, Marc Tramier. Real-Time Monitoring of Aurora kinase A Activation using Conformational FRET Biosensors in Live Cells. *Journal of visualized experiments: JoVE*, 2020, 161, 10.3791/61611 . hal-02929723

**HAL Id: hal-02929723**

**<https://hal.science/hal-02929723>**

Submitted on 25 Nov 2020

**HAL** is a multi-disciplinary open access archive for the deposit and dissemination of scientific research documents, whether they are published or not. The documents may come from teaching and research institutions in France or abroad, or from public or private research centers.

L'archive ouverte pluridisciplinaire **HAL**, est destinée au dépôt et à la diffusion de documents scientifiques de niveau recherche, publiés ou non, émanant des établissements d'enseignement et de recherche français ou étrangers, des laboratoires publics ou privés.

1  
2  
3  
4  
5  
6  
7  
8  
9  
10  
11  
12  
13  
14  
15  
16  
17  
18  
19  
20  
21  
22  
23  
24  
25  
26  
27  
28  
29  
30  
31  
32  
33  
34  
35  
36  
37  
38  
39  
40  
41  
42  
43  
44

**TITLE:**

Real-time monitoring of Aurora kinase A activation using conformational FRET biosensors in live cells.

**AUTHORS AND AFFILIATIONS:**

Giulia Bertolin<sup>1</sup>, Gilles Le Marchand<sup>1</sup>, and Marc Tramier<sup>1</sup>

<sup>1</sup>Univ Rennes, CNRS, IGDR (Genetics and Development Institute of Rennes), UMR 6290, F-35000 Rennes, France

**CORRESPONDING AUTHORS:**

Giulia Bertolin ([giulia.bertolin@univ-rennes1.fr](mailto:giulia.bertolin@univ-rennes1.fr)); Marc Tramier ([marc.tramier@univ-rennes1.fr](mailto:marc.tramier@univ-rennes1.fr))

**KEYWORDS:**

AURKA, FRET, FLIM, genetically-encoded biosensors, conformational change, activation, mitosis, live cells.

**SUMMARY:**

The activation of the multifunctional Ser/Thr kinase AURKA is hallmarked by its autophosphorylation on Thr288. Fluorescent probes relying on FRET allow to discriminate between its inactive and activated states. We here illustrate some strategies for probe engineering, together with a rapid FRET protocol to follow the kinase activation throughout mitosis.

**ABSTRACT:**

Epithelial cancers are often hallmarked by the overexpression of the Ser/Thr kinase Aurora A/AURKA. AURKA is a multifunctional protein which activates upon its autophosphorylation on Thr288. AURKA abundance peaks in mitosis, where it controls the stability and the fidelity of the mitotic spindle, and the overall efficiency of mitosis. Although well characterized at the structural level, a consistent monitoring of the activation of AURKA throughout the cell cycle is lacking. A possible solution consists in using genetically-encoded Förster’s Resonance Energy Transfer (FRET) biosensors to gain insight into the autophosphorylation of AURKA with sufficient spatiotemporal resolution. Here, we describe a protocol to engineer FRET biosensors detecting Thr288 autophosphorylation, and how to follow this modification during mitosis. First, we provide an overview of possible donor/acceptor FRET pairs, and we show possible cloning and insertion methods of AURKA FRET biosensors in mammalian cells. Then, we provide a step-by-step analysis for rapid FRET measurements by Fluorescence Lifetime Imaging Microscopy (FLIM)

45 on a custom-built setup, which has recently been released to the market by Inscoper. However,  
46 this protocol is also applicable to alternative commercial solutions available. We conclude by  
47 considering the most appropriate FRET controls for an AURKA-based biosensor, and by  
48 highlighting potential future improvements to further increase the sensitivity of this tool.

49

## 50 INTRODUCTION:

51

52 Aurora kinase A/AURKA is a multifunctional serine/threonine kinase, active throughout the cell  
53 cycle and at different subcellular compartments <sup>1</sup>. Understanding its broad spatiotemporal  
54 activation is particularly important in cancer, as AURKA is often overexpressed in epithelial and  
55 hematological malignancies, with patients showing poor responsiveness to the currently-  
56 available therapies <sup>2</sup>.

57 Structural studies revealed that AURKA undergoes two steps to convert from an inactive to an  
58 active kinase. First, the autophosphorylation of Thr288 changes the conformation of the kinetic  
59 pocket of the kinase and activates it <sup>3-6</sup>. This step increases the catalytic activity of AURKA in  
60 human cells and in *Xenopus laevis* <sup>3,6,7</sup>, “priming” the kinase for full activity. Once activated, the  
61 interaction of AURKA with the Targeting Protein for Xklp2 (TPX2) induces a second  
62 conformational change <sup>5</sup>. This further modification allows AURKA to reach a full enzymatic  
63 activity towards its substrates in the cell <sup>5,8-10</sup>.

64

65 For nearly two decades, insights on the activation and activity of AURKA were obtained mainly  
66 with a combination of biochemical approaches. These include the detection of phosphorylated  
67 Thr288 in cells or *in vivo* as a hallmark of AURKA activation, crystallography analyses, and *in vitro*  
68 or *in cellulo* kinase assays to probe the activity of AURKA <sup>1</sup>. However, the spatiotemporal  
69 resolution of these approaches is poor or absent, and novel solutions were needed to broaden  
70 our knowledge of the dynamics of these two events.

71

72 The development of fluorescent probes in the last years facilitated the monitoring of AURKA in  
73 live cells, allowing to follow its activation with greater spatiotemporal resolution. The most  
74 specific sensors for AURKA developed so far rely on the principle of FRET (Förster’s Resonance  
75 Energy Transfer) <sup>11</sup> to discriminate between inactive and active – autophosphorylated – AURKA.  
76 The first sensor developed was a substrate-based biosensor of AURKA kinase activity. Substrate-  
77 based biosensors are constituted by a short aminoacidic sequence targeted by a given kinase for  
78 phosphorylation, and inserted within a donor/acceptor FRET pair and a binding domain  
79 recognizing the phosphorylated residue, which helps the folding of the biosensor for an efficient  
80 FRET process <sup>12</sup>. In the case of AURKA, a 14-aminoacid fragment of KIF2C targeted by  
81 phosphorylation was inserted between a CFP-YFP donor/acceptor pair <sup>13</sup>. However, this sensor  
82 has some major drawbacks. First, the KIF2C sequence used in this probe can be targeted both by  
83 AURKA and the closely-related kinase AURKB, thereby decreasing the specificity of this biosensor.  
84 Second, the sensor relies on the endogenous kinase for phosphorylation. Therefore, FRET  
85 efficiency can be undetectable or not significant if the quantities of the kinase are limiting e.g. in  
86 subcellular compartments or cell cycle phases. To overcome these limitations, a new class of  
87 AURKA sensor was created known as “conformational sensors”. In these probes, the full-length  
88 sequence of AURKA was inserted within a donor fluorophore at the N-terminus, and an acceptor

89 fluorophore at the C-terminus. Inactive AURKA presents an “open” conformation, which brings  
90 the N- and C-termini of the kinase away from each other. With such distance between the two  
91 termini (> 10 nm), the donor/acceptor pair are at a non-permissive configuration for FRET. On  
92 the contrary, autophosphorylated AURKA adopts a “closed” conformation, with the two protein  
93 termini and the two fluorophores in proximity. This was shown to allow FRET between the donor  
94 and the acceptor, which can be measured using the variations in the donor lifetime<sup>14, 15</sup>. Such  
95 probes present several advantages. First, they are genetically-encoded, and they can be used to  
96 replace the endogenous kinase in the cell. Second, they rescue the phenotypes induced by the  
97 knockdown of AURKA, indicating that they are functional in the cell. Third, they allow to follow  
98 the activation of the kinase at different subcellular compartments and throughout the cell cycle.  
99 Not only they detected the activation of AURKA at locations where the kinase is known to be  
100 activated (i.e. centrosomes and the mitotic spindle), but they also participated in discovering the  
101 activation of AURKA at mitochondria<sup>16</sup>. Last, these sensors allowed high-content screenings  
102 based on FRET/FLIM, where the conformational changes of AURKA were used to identify novel  
103 pharmacological inhibitors<sup>17</sup>.

104  
105 In the present work, we describe a procedure to visualize AURKA activation in cultured cells. First,  
106 we will make an insight on potential fluorophore pairs for FRET. The choice of the most suitable  
107 donor/acceptor pair will be made according to the available microscope setup, or a particular  
108 downstream application as multiplex FRET<sup>18, 19</sup>. Then, we propose a pipeline to explore the  
109 behavior of the biosensor(s) chosen in a rapid FRET/FLIM microscope setup. This pipeline will  
110 extend from cell culture and synchronization procedures to FLIM acquisition and data analysis.  
111 Last, we will discuss the potential advantages of this protocol, as an analogous strategy for  
112 biosensor design could be applied to other kinases, and it may also be used with other FRET-  
113 based imaging systems.

## 114 115 **PROTOCOL:**

116  
117 U2OS cells used in this protocol were purchased from American Type Culture Collection (ATCC,  
118 HTB-96), and they were tested free from mycoplasma. Step 2.1 to 2.7 should be performed under  
119 a laminar flow hood to keep cells and reagents sterile.

### 120 121 **1. Choosing the donor/acceptor FRET pair**

122  
123 1.1 Refer to the literature for the choice of the most suitable donor/acceptor FRET pairs. Useful  
124 examples can be found in<sup>20-24</sup>, although the final choice must be made according to the  
125 characteristics of the FRET/FLIM setup (available laser lines, filters etc...). Some  
126 considerations on how to select a donor/acceptor pair are:

127  
128 1.1.1 **Choosing the donor:** refer to the FP base (<https://www.fpbases.org/>) for a complete set  
129 of information on the available fluorescent proteins. This database is constantly updated  
130 with all the newly-developed fluorophores.

131  
132 1.1.2 Also refer to the Fluorescent Biosensor Database

133 (<https://biosensordb.ucsd.edu/index.php>) for more information on the biosensors  
134 already available in the literature, together with the respective fluorescent proteins  
135 used.

136

137 1.1.3 As a general starting point, choose a bright donor fluorophore. Good candidates are cyan  
138 fluorescent proteins as mTFP1 or ECFP, or GFP variants as EGFP or mEGFP.

139

140 1.1.4 Oligomers can affect protein localization and/or function<sup>25</sup>. Consider using monomeric  
141 mutants of CFP as mTurquoise2<sup>26</sup>, or Aquamarine<sup>27, 28</sup>. These variants also have good  
142 quantum yield and extinction coefficients, which make them good candidates as FRET  
143 donors.

144

145 1.1.5 Preference should be given to fluorescent proteins (both as donor or acceptors)  
146 insensitive to environmental changes like intracellular pH<sup>23</sup>, or to photobleaching<sup>25</sup>, as  
147 FRET efficiency can be heavily affected by these parameters<sup>29</sup>.

148 Nowadays, fluorophores like mTurquoise2 or mTFP1 are extensively used as donors,  
149 thanks to their good photostability<sup>22, 25, 26</sup>.

150

151 1.2 **Choosing the acceptor:** cyan donors are often paired with Yellow Fluorescent Protein (YFP)  
152 variants, as mVenus, Citrine, and YPet<sup>20-22, 30</sup>. However, it should be noted that these  
153 proteins have a much greater sensitivity to pH, and globally display a poor photostability.

154

155 1.2.1 Consider using newly-developed, pH-insensitive yellow variants of YFP as pH-Lemon<sup>31</sup>,  
156 green fluorophores as mNeonGreen<sup>23</sup> or red fluorophores as mScarlet-I<sup>23, 32</sup> as  
157 previously-validated fluorescent acceptors for mTurquoise2.

158

159 1.2.2 Alternatively, consider using non-fluorescent/dark derivatives of YFP as ShadowG<sup>33</sup> or  
160 ShadowY<sup>34</sup>, which were shown to behave as good acceptors for cyan-fluorescent donors  
161 in FRET/FLIM experiments.

162

163 1.2.3 If using mEGFP as a donor, consider using monomeric red acceptors as mCherry.

164

165 1.3 Verify the spectral properties of the chosen donor/acceptor pair using the tools available  
166 on the FP base website. See Figure 1 for an example of the mEGFP/mCherry pair.

167

168 1.3.1 On the FP base website, enter in the “Tools” drop-down menu and select “Spectra  
169 viewer”;

170

171 1.3.2 In the drop-down menus, enter the name of the fluorophore pair to visualize e.g. mEGFP  
172 and mCherry;

173

174 1.3.3 Simulate the properties of the donor/acceptor pair with a specific light source by  
175 selecting a given laser in the drop-down menu. Alternatively, enter a specific laser  
176 wavelength by selecting “Add laser”. Click on the “Normalize emission to this” option to

177 adjust the fluorophore spectra to the desired wavelength. E. g. on our system, the  
178 wavelength used to excite GFP is at  $480 \pm 10$  nm.

179  
180 1.4 Clone the selected donor/acceptor pair by adding one fluorophore at the N-terminus of the  
181 full-length sequence of AURKA, and one at the C-terminus. Follow the guidelines of your  
182 preferred cloning method to insert this construct in a mammalian expression vector of  
183 choice.

## 184 185 **2. Cell culture, transfection and synchronization.**

186  
187 2.1 **DAY 1.** Prepare culture medium for U2OS cells: use Dulbecco's Modified Eagle Medium  
188 (DMEM) supplemented with 10% Fetal Bovine Serum (FBS), 1% Penicillin-Streptomycin and  
189 1% L-Glutamine (from here on, *Complete growth media*). Alternatively, DMEM with pre-  
190 supplemented L-Glutamine can also be used.

191  
192 2.2 If cells are frozen, thaw a vial at least 8 days prior to experiments (i.e. From point 2.5 on).

193  
194 2.3 Grow cells in an incubator dedicated to mammalian cell cultures, at  $37^{\circ}\text{C}$  and with 5%  $\text{CO}_2$ .  
195 Clean and sterilize the incubator regularly to avoid contaminations.

196  
197 2.4 When the cells reach  $\sim 80\%$  confluence:

198  
199 2.4.1 Wash them briefly with sterile 1X Phosphate Buffer Saline (PBS) without  $\text{Ca}^{2+}$  and  $\text{Mg}^{2+}$   
200

201 2.4.2 Trypsinize cells with sterile 0.05% Trypsin-EDTA and by placing cells in the incubator for  
202 1-3 min.

203  
204 2.4.3 Inactivate Trypsin by adding twice the volume of complete growth media; mix well.

205  
206 2.4.4 Centrifuge the cell suspension at 800g for 3-5 min.

207  
208 2.4.5 Count the cells using a hemocytometer, and calculate the appropriate dilution for them  
209 to be at  $\sim 70\text{-}80\%$  confluency in LabTek Chamber Slides the day after. Alternatively, similar  
210 supports for live cell imaging can also be used.

211  
212 2.4.6 Pipet the corresponding volume of cells in the chosen live cell imaging support, and place  
213 cells back in the incubator until the day after.

214  
215 2.5 **DAY 2.** Proceed with transfection. Follow the guidelines of your preferred transient  
216 transfection method(s) to obtain an optimal transfection efficiency ( $\sim 50\text{/}80\%$ ). No specific  
217 transfection method is required. Note that the transfection efficiency may vary according to  
218 the cell line used. Incubate for 48 h.

219 **NOTE:** you can also produce stable clones containing each of the three vectors to bypass the  
220 need of transient transfections.

221 **NOTE:** at this stage, two types of controls should be planned. First, a “donor-only” control is  
222 required to verify that the presence of full-length AURKA does not perturb the lifetime of  
223 mTurquoise2 *per se*. Second, a biosensor carrying a kinase-dead mutation should be used as a  
224 negative control where FRET is abolished or significantly lowered. Alternatively to a kinase-dead  
225 mutant, a chemical inhibitor of AURKA activation as the ATP analog MLN8237 can be used as a  
226 negative control.

227

228 2.5.1 Plan ahead three transfection conditions, each of them in an independent well:

229 - The “donor-only” vector: e.g. AURKA-mTurquoise2

230 - The “biosensor”: e.g. superYFP-AURKA-mTurquoise2

231 - A kinase-dead/“K162M” biosensor: e.g. superYFP-AURKA K162M-mTurquoise2 or  
232 alternatively, an inhibitor of AURKA activation (e.g. MLN8233)

233

234 2.5.2 These three conditions should be carried out for each independent donor/acceptor pair  
235 you wish to compare.

236

237 2.5.3 Consider doubling the number of transfected wells if you wish to compare  
238 unsynchronized and G2/M-synchronized cells (see point 2.6).

239

240 2.6 **DAY 3.** Synchronize cells in G2/M. Add 100 ng/ml Nocodazole dissolved in DMSO to each  
241 transfected well avoiding light exposure, and incubate for 16 h (preferably overnight). If you  
242 wish to compare unsynchronized and G2/M-synchronized cells, each transfection condition  
243 should be treated with Nocodazole or with an equal volume of DMSO. For a better  
244 synchronization efficiency, prepare single-use aliquots of Nocodazole in DMSO, store them  
245 at -20°C and discard them after use.

246 **NOTE:** cell synchronization efficiency can vary among cell lines. The optimal  
247 concentration of nocodazole and its incubation time should be experimentally determined  
248 by flow cytometry approaches prior to FRET/FLIM experiments. For statistically-relevant  
249 FRET/FLIM analyses, we recommend a synchronization efficiency in G2/M of at least 50% of  
250 the overall cell population.

251

252 2.7 **DAY 4.** Nocodazole washout and FRET/FLIM imaging on mitotic cells

253

254 2.7.1 Remove the culture medium with a pipette and replace it with pre-warmed, sterile PBS.  
255 Avoid light exposure if possible. Gently rock the plate.

256

257 2.7.2 Repeat the washing procedure, always avoiding light exposure.

258

259 2.7.3 Remove the second PBS washing and replace it with pre-warmed, sterile Leibovitz L-15  
260 medium, supplemented with 20% Fetal Bovine Serum (FBS) and 1% Penicillin-  
261 Streptomycin (from here on, *Imaging media*).

262 **NOTE:** Imaging media should be purchased without pH indicators (e.g. phenol red) and  
263 medium components as riboflavin. These substances are a source of autofluorescence  
264 which could perturb lifetime values.

265  
266 2.7.4 Proceed with FRET/FLIM imaging. Minimize rapid changes in temperature and proceed  
267 to the imaging step (See point 3) as fast as possible. Consider protecting the sample  
268 from light while transporting it to the microscope setup, i.e. by wrapping it in an  
269 aluminum foil or placing it in a box.

270  
271  
272

### 273 3. FRET/FLIM acquisitions

274

275 To ensure an optimal release of cells from the G2/M block into mitosis, experiments should be  
276 performed at 37°C. If possible, perform FRET/FLIM experiments with microscope setups  
277 equipped with a thermostatic chamber.

278

279 **NOTE:** FRET/FLIM acquisitions in this protocol were performed on a custom-built setup,  
280 described in <sup>35</sup> and equipped with the Inscoper control solution as in <sup>15,17</sup> (Figure 2). The setup is  
281 now commercialized by Inscoper and it is made of a spinning-disk microscope with a white laser  
282 for pulsed excitation, and a high-rate time-gated intensifier in front of the camera. Temporal  
283 gates of 2 nsec in a time window of 10 nsec are sequentially used to obtain a stack of five time-  
284 gated images. These images are then used to calculate the pixel-by-pixel mean fluorescence  
285 lifetime according to the following equation:  $\tau = \frac{\sum \Delta t_i \cdot I_i}{\sum I_i}$ , where  $\Delta t_i$  corresponds to the  
286 delay time of the of the  $i^{\text{th}}$  gate while  $I$  indicates the pixel-by-pixel time-gated intensity image <sup>35</sup>,  
287 <sup>36</sup>. This method ensures rapid FLIM measurements: no fitting or binning steps are required, and  
288 lifetime can be calculated in an online mode, with minimal photon budget. The system also  
289 presents a user-friendly software interface. However, the **same experiment can be performed**  
290 **under any other commercial microscope setup equipped for FLIM measurements.**

291

292 3.1 Turn on the thermostatic chamber of the microscope at least 30 min to 1 h before the  
293 experiment.

294

295 3.2 Switch on the laser, the camera, the microscope setup and the imaging software (Figure 2).

296

297 3.3 Select the appropriate excitation and emission wavelengths for the donor fluorophore.  
298 Convenient wavelengths options are:  $\lambda_{\text{ex}}$  440/10 nm and  $\lambda_{\text{em}}$  483/35 nm for mTurquoise2  
299 (Figure 3A);  $\lambda_{\text{ex}}$  488/10 nm and  $\lambda_{\text{em}}$  525/50 nm for GFP) (Figure 3B).

300

301 3.4 Set the exposure time, generally between 30 and 100 msec (Figure 3). Beware that excessive  
302 laser power may result in induced phototoxic effects as photobleaching, which could in turn  
303 modify the fluorescence lifetime <sup>37</sup>. On the Inscoper setup, validate the absence of  
304 photobleaching events by monitoring the fluorescence intensity of the first gate during time-  
305 lapse acquisitions. If variations in the fluorescence intensity are observable, discard the  
306 acquisition and adjust laser power.

307 **NOTE:** on the Inscoper setup, select an exposure time allowing you to have at least 3000 gray  
308 levels in the first gate, otherwise the software will not calculate donor lifetime. This gray

309 level value corresponds to the minimal photon budget necessary to obtain relevant lifetime  
310 values.

311  
312 3.5 Before launching FRET/FLIM acquisitions Ensure that cells have entered mitosis, by waiting  
313 until the appearance of the bipolar spindle (~20/30 min in U2OS cells). Since mitotic AURKA  
314 localizes mainly at this structure, mitotic progression can be verified by screening the  
315 formation of the spindle in cells directly under the microscope, with an external light source  
316 (Figure 1). Note that the time required for mitotic progression might vary according to the  
317 cell line used.

318  
319 3.6 If treatment with MLN8237 is planned, place the cells under the microscope and allow them  
320 to reach metaphase (approx. 20 min after Nocodazole washout). Add 250 nM MLN8237  
321 dissolved in DMSO both to cells expressing the donor-only construct and to cells expressing  
322 the biosensor. This condition should be controlled on cells transfected as above, and  
323 incubated with an equal volume of DMSO. For a better AURKA inhibition, prepare single-use  
324 aliquots of MLN8237 in DMSO, store them at -80°C. Thaw them by placing the aliquots on  
325 ice, and discard them after use. Incubate for 10 min. After this period, the mitotic spindle  
326 will shrink and only a single, intense dot is left. A similar phenotype is observed when  
327 Lys162Met mutants are used.

328  
329 3.7 For a better resolution of the mitotic spindle, use at least a 63x objective (Figure 3).

330  
331 3.8 Once found a cell in metaphase (See Figure 4 as an example of a cell in metaphase), adjust  
332 xyz coordinates to place it at the center of the field of view.

333  
334 3.9 For faster images, select one single z plan. Choose the plan where the mitotic spindle is more  
335 visible or intense.

336  
337 3.10 Start the recording. The acquisition time may vary according to the FLIM setup used (from  
338 few sec to min). The majority of the commercial setups available on the market will elaborate  
339 both the fluorescence micrograph and the pixel-by-pixel lifetime map. Save both images.

340  
341 3.11 Acquire at least 10 independent images from each transfection and/or treatment condition.

342  
343 **4. Calculation of  $\Delta$ Lifetime and comparison of FLIM values among donor/acceptor pairs**

344  
345 4.1 Extract lifetime values from the whole pixel-by-pixel lifetime map (i.e. the entire mitotic  
346 spindle), or select Regions of Interest (ROIs) corresponding to specific subregions.

347 **NOTE:** According to the FRET/FLIM setup used, lifetime calculations may be performed  
348 directly on the acquisition software, or extracted with generic image processing solutions  
349 (e.g. Fiji/ImageJ: <https://fiji.sc/>). Software directly calculating lifetime values (also known as  
350 *online mode*) offer a more user-friendly solution, which is suitable for beginners and for  
351 microscopy users not fully familiar with FRET/FLIM. On the contrary, the extraction of  
352 lifetime values after acquisition often requires a fitting procedure. This option is less

353 accessible to beginners, as some previous knowledge on mathematical models of fitting is  
354 necessary.

355  
356 4.2 Once visualized or extracted, calculate the mean lifetime of the cells expressing the “donor-  
357 only” vector (e.g. AURKA-mTurquoise2), hereby *mean donor lifetime*.

358  
359 4.3 Subtract each independent lifetime value calculated in step 4.1 from the mean donor  
360 lifetime. Repeating this step for all cells in all conditions analyzed will give the  $\Delta$ Lifetime for  
361 every condition.

362  
363 4.4 Compare  $\Delta$ Lifetime values for the “donor-only”, the “biosensor” and the “K162M”, or the  
364 DMSO and the MLN8237 conditions.

365 **NOTE:** For the “donor-only” condition,  $\Delta$ Lifetime should result in values close to zero and  
366 corresponding to the experimental fluctuations of lifetime values. For the “biosensor”  
367 condition,  $\Delta$ Lifetime values should yield the net difference between the two constructs (see  
368 Figure 4 for an illustrated example).

369  
370 4.5 Compare  $\Delta$ Lifetime values among different donor/acceptor pairs:

371  
372 4.5.1 Compare the “biosensor” conditions: do they show similar  $\Delta$ Lifetime?

373  
374 4.5.2 Do the “K162M” or the MLN8237 conditions show similar  $\Delta$ Lifetime among them? Is their  
375  $\Delta$ Lifetime similar to the “donor-only” condition?

376  
377 **REPRESENTATIVE RESULTS:**

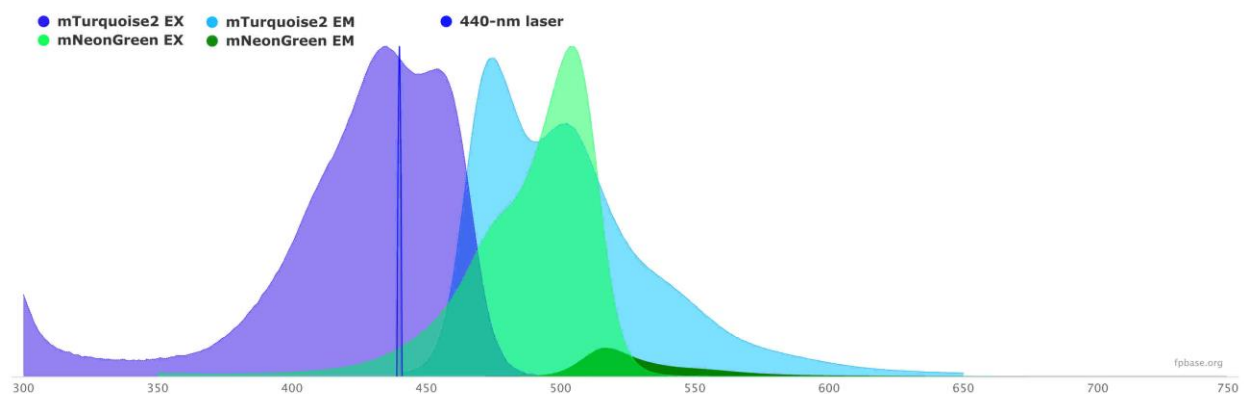
378  
379 We followed the procedure described above to record the autophosphorylation of AURKA on  
380 Thr288 using two biosensors with different spectral properties. We compared our initial GFP-  
381 AURKa-mCherry probe <sup>14</sup> with two biosensors with different spectral properties. These two  
382 probes rely on the fluorescent donor mTurquoise2 and on a non-fluorescent acceptor (ShadowG)  
383 in one case, or a yellow acceptor (superYFP) in a second case. We then inserted the full-length  
384 sequence of AURKA within each donor/acceptor pair. To have a negative control for AURKA  
385 activation, two strategies can be pursued. First, the use a small ATP-analog – MLN8237 –  
386 interferes with the binding of ATP in the kinetic pocket of the kinase and prevents its activation  
387 <sup>38</sup>. Second, the mutation of Lys162 into Met (K162M), creates a kinase-dead version of each  
388 biosensor incapable of activating <sup>14, 15, 39</sup>. This mutation induces the disruption of a salt bridge  
389 normally established between Lys162 and Glu181, which results in a stable opening of the kinetic  
390 pocket of the kinase and which triggers its overall inactivation <sup>40</sup>. As a negative control for FRET,  
391 we used an acceptor-devoid construct – GFP-AURKA or AURKA-mTurquoise2 –.

392  
393 After synchronizing cells in G2/M and releasing them into mitosis, we measured the lifetime of  
394 all the transfected constructs at the mitotic spindle (Figure 4). Of note, this structure was  
395 considered as a whole, and no ROIs within the spindle were analyzed. We then calculated

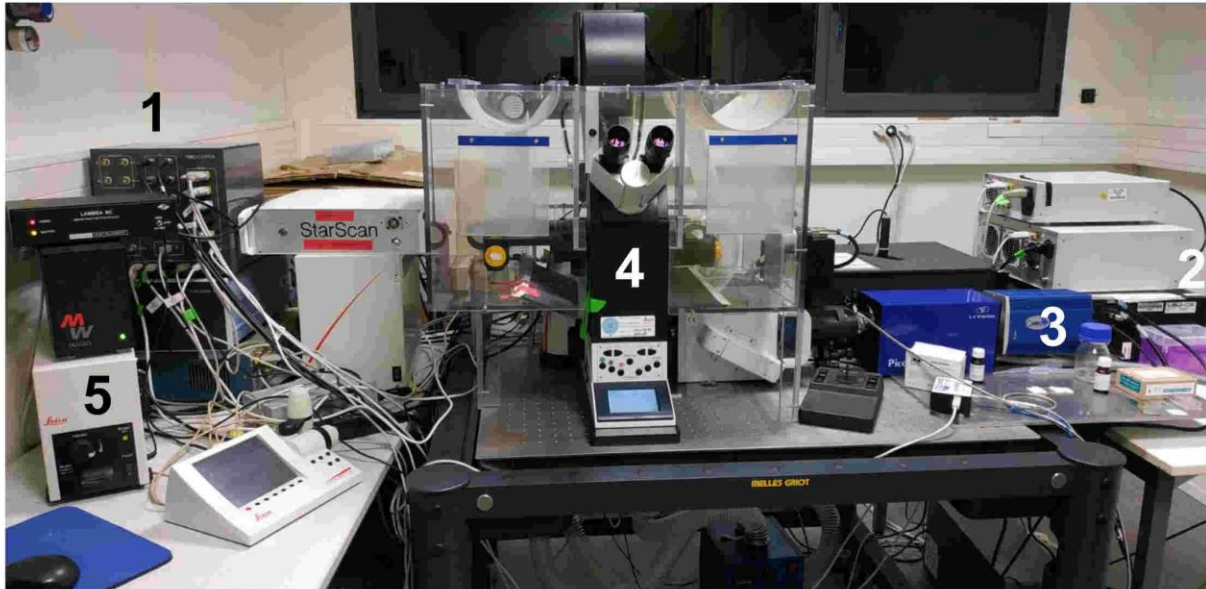
396  $\Delta$ Lifetime for all conditions. As expected, the lifetime of GFP-AURKA or AURKA-mTurquoise2 –  
397 the “donor-only” conditions – was close to 0, indicating that the values measured for these  
398 constructs fluctuated around the mean value (Figure 4A and B). Conversely, the  $\Delta$ Lifetime values  
399 for GFP-AURKA-mCherry were statistically different from the donor-only condition, with  
400  $\Delta$ Lifetime increasing of  $\sim 130$  psec (Figure 4A). Similar observations were made for shadowG-  
401 AURKA-mTurquoise2 and for superYFP-AURKA-mTurquoise2, with  $\Delta$ Lifetime increasing of  $\sim 150$   
402 and  $\sim 220$  psec from the donor-only condition, respectively (Figure 4B and C). These data can be  
403 easily visualized in single cells with a pseudocolor Lookup Table (LUT). In this case, values of  
404  $\Delta$ Lifetime around 0 are pseudocolored yellow, while more significant differences are  
405 pseudocolored red/purple. Indeed, the pixel-by-pixel LUT was closer to yellow in cells expressing  
406 the donor-only constructs, while it was more in the red/purple spectrum in cells expressing either  
407 biosensor (Figure 4A and B). This was also observed when the GFP-AURKA-mCherry biosensor  
408 was treated with the pharmacological inhibitor MLN8237.  
409

410 We then analyzed the  $\Delta$ Lifetime of kinase-dead biosensors. These constructs showed  
411 intermediate  $\Delta$ Lifetime values:  $\Delta$ Lifetime was significantly higher when compared to the donor-  
412 only condition (Figure 4B and C), but it was also significantly lower than their normal counterparts  
413 (Figure 4B and D). The comparisons with cells treated with MLN8237 or expressing kinase-dead  
414 biosensors are necessary to estimate whether  $\Delta$ Lifetime variations for each donor/acceptor pair  
415 are solely linked to the activation of AURKA. In the case of GFP-AURKA-mCherry,  $\Delta$ Lifetime  
416 variations are abolished when an AURKA-specific inhibitor is used. Conversely,  $\Delta$ Lifetime  
417 variations are mostly, but not exclusively linked to AURKA activation in the case of shadowG-  
418 AURKA-mTurquoise2 and of superYFP-AURKA-mTurquoise2.  
419

#### 420 FIGURE LEGENDS:

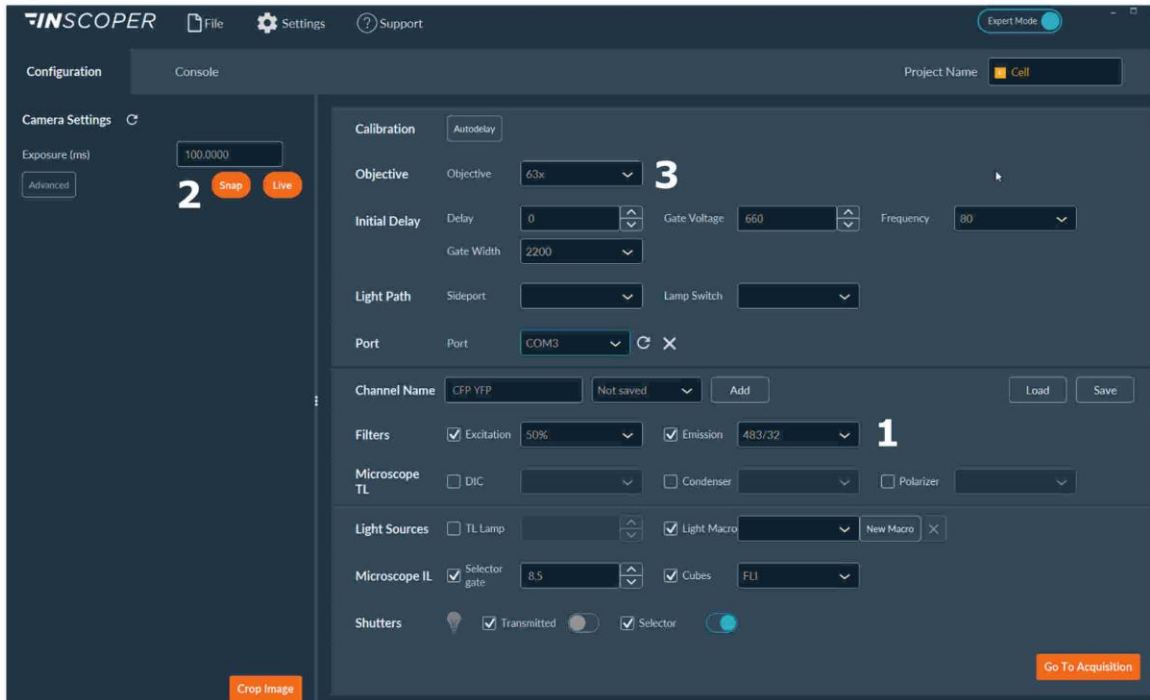


421  
422 **Figure 1. GFP (donor) and mCherry (acceptor) excitation and emission spectra.** Spectra were  
423 obtained and adapted from the FP base website (<https://www.fpbase.org/>), and adjusted to a  
424 480 nm-laser excitation.  
425

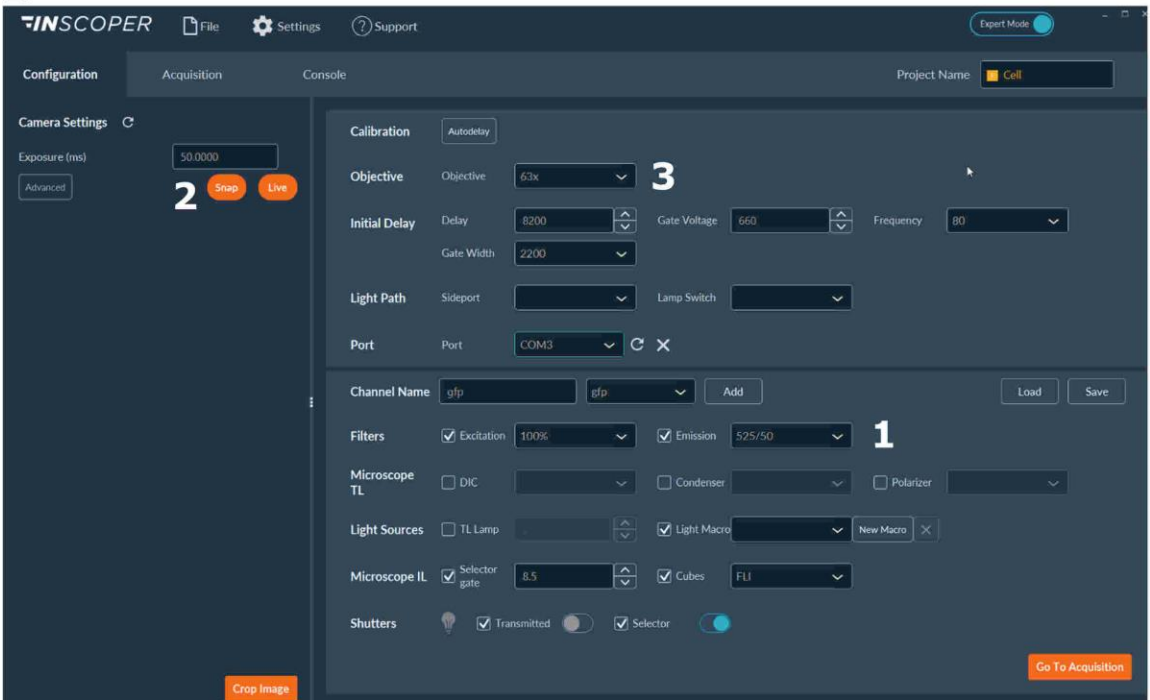


427 **Figure 2. Image of the experimental workspace.** (1) Inscoper control solution; (2) white laser  
428 source; (3) CCD camera; (4) microscope setup; (5) external light source/lamp for ocular screening  
429 of the sample.  
430

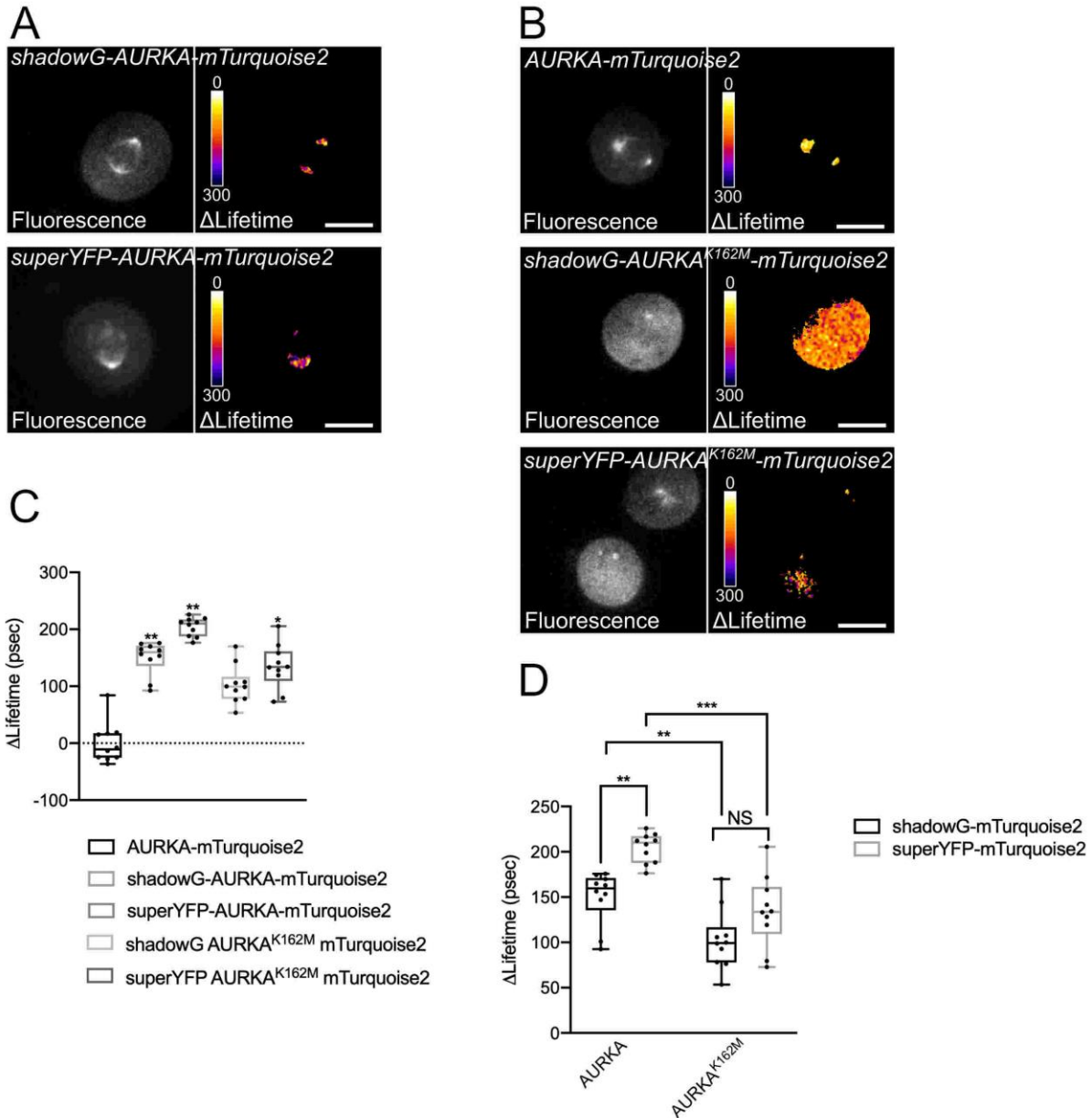
A



B



432 **Figure 3. Representative images of the Inscoper software for FLIM acquisition. (A, B) (1)**  
 433 **excitation and emission parameters for the donor (CFP in A, or GFP in B); (2) exposure time; (3)**  
 434 **selection of the objective.**  
 435



436 **Figure 4. Representative images of AURKA FRET biosensors and their negative controls. (A)**  
 437 **(Micrographs) Fluorescence (green channel) and corresponding pixel-by-pixel  $\Delta$ Lifetime (donor**  
 438 **only – biosensor) of U2OS cells expressing GFP-AURKA or GFP-AURKA-mCherry, synchronized at**  
 439 **G2/M, released until the bipolar spindle is visible and then treated with DMSO or with MLN8237.**  
 440  **$\Delta$ Lifetime is illustrated with a pseudocolor scale (“Fire” lookup table). (Graph) Corresponding**  
 441 **quantification and two-way ANOVA analysis for the indicated conditions. (B) (Micrographs)**  
 442

443 Fluorescence (cyan channel) and corresponding pixel-by-pixel  $\Delta$ Lifetime (donor only – biosensor)  
444 of U2OS cells expressing shadowG-AURKA-mTurquoise2 (upper panel) or superYFP-AURKA-  
445 mTurquoise2 (lower panel), synchronized at G2/M and released until the bipolar spindle is visible.  
446  $\Delta$ Lifetime is illustrated with a pseudocolor scale (“Fire” lookup table). (Graph) Corresponding  
447 quantification and one-way ANOVA analysis of conditions represented in the above micrographs.  
448 **(C)** (Micrographs) Images of AURKA-mTurquoise2 (upper panel), shadowG-AURKA K162M-  
449 mTurquoise2 (middle panel) and superYFP-AURKA K162M-mTurquoise2 acquired and  
450 represented as in the micrographs. (Graph) Two-way ANOVA analysis for the indicated  
451 transfection conditions. The bar in boxplots represents the median; whiskers extend from the  
452 min to the max.  $n = 10$  cells per condition of one representative experiment (of three). Individual  
453 values are represented as dots. Scale bar: 10  $\mu$ m. \* $P < 0.05$ , \*\* $P < 0.01$ , \*\*\* $P < 0.001$  against each  
454 indicated condition in (A) the “AURKA-mTurquoise2” condition in (B), and against each indicated  
455 condition in (C). NS: not significant.

456

## 457 **DISCUSSION:**

458

459 Genetically-encoded FRET biosensors are reliable tools to measure the activation of single  
460 proteins or of entire signaling pathways<sup>41</sup>. Particularly, the AURKA FRET biosensor constitutes a  
461 preferential way to explore the activation of the kinase in time and space. However, some  
462 elements deserve special attention when designing or optimizing a FRET biosensor, not only in  
463 general terms but more specifically for AURKA.

464

465 First, the nature and the relative position of the donor/acceptor FRET pair can be adapted for  
466 specific functions of this kinase. AURKA is greatly enriched at the mitotic spindle during mitosis,  
467 but it is present throughout the cell cycle and at different subcellular locations as centrosomes,  
468 the nucleus and mitochondria<sup>1, 2</sup>. If the biosensor is to be used in specific compartments like  
469 mitochondria – which can reach acidic pH – the choice of a pH-insensitive donor-acceptor FRET  
470 pair as mTurquoise2/shadowG should be made. Moreover, placing the FRET donor at the C-  
471 terminus could allow a better visualization of the biosensor at this subcellular compartment, and  
472 potentially even optimize FRET detection given that AURKA N-terminus was shown to partially  
473 cleave off at mitochondria<sup>16, 42</sup>.

474

475 Second, a yet unexplored way of optimizing the AURKA FRET biosensor would require a more  
476 careful design of linkers between full-length AURKA and the donor/acceptor pair. Not only the  
477 distance between the fluorescent pair, but also the properties of the linker itself were shown to  
478 be key factors to improve FRET efficiency<sup>43-46</sup>. In this light, increasing the rigidity or the flexibility  
479 of the linker could either be detrimental to FRET efficiency, or further improve it.

480

481 Third, it is known that the overexpression of AURKA induces mitotic spindle abnormalities in a  
482 significant proportion of cells<sup>2</sup>. It would be interesting to compare  $\Delta$ Lifetime obtained by  
483 expressing the same FRET construct under a strong promoter like cytomegalovirus (CMV) – one  
484 of the most common promoters found in mammalian expression vectors – or under the AURKA  
485 minimal promoter sequence (CTTCCGG)<sup>14, 47</sup>. This promoter was previously shown to rescue  
486 monopolar or multipolar spindles arising after the knock-down of the kinase, and its use did not

487 induce cell cycle perturbations *per se*<sup>14, 47</sup>. Although FLIM is insensitive to protein expression  
488 levels and relative concentrations in the cell<sup>11</sup>, benefiting from a thorough comparison of the  
489 two promoters on the same biosensor setup would broaden our understanding of the pool of  
490 activated AURKA at any given location. In addition, it would provide novel insights on how AURKA  
491 activation may change upon overexpression, which is relevant for epithelial and hematologic  
492 cancer paradigms.

493  
494 Last, the downstream FRET application should also be taken into account. A future perspective  
495 in the field of AURKA would be to cumulate the kinase conformational biosensor with a substrate-  
496 based biosensor. Analyzing the FRET behavior of two biosensors simultaneously – a process  
497 known as multiplex FRET – requires a dark acceptor on the first biosensor to avoid spectral bleed  
498 through in the second donor channel. In the context of AURKA, this would open up the exciting  
499 new perspective of detecting the activation of the kinase with the first biosensor, and its  
500 enzymatic activity towards a given substrate with the second one. Recent developments in  
501 multiplexing now allow to cumulate up to three biosensors at a time<sup>48</sup>. Applying a similar method  
502 in the context of AURKA could represent a very promising strategy not only to test the activation-  
503 activity interplay of the kinase, but also to explore AURKA signaling cascades with unprecedented  
504 spatiotemporal resolution.

505  
506 In conclusion, FRET/FLIM is a convenient way to deepen our knowledge on protein activity. On  
507 one hand, it allows to visualize the localization of a given protein in live cells, thanks to at least  
508 one fluorescent moiety. On the other hand, it can unravel protein conformational changes, which  
509 could be informative on protein activation and/or activity. Therefore, FRET/FLIM and  
510 conformational FRET biosensors have the potential of becoming widespread methods to follow  
511 signaling pathways in live cells, and with exquisite spatiotemporal resolution.

#### 512 513 **ACKNOWLEDGMENTS:**

514  
515 We thank the engineers of the Microscopy-Rennes Imaging Center (MRic, BIOSIT, Rennes, France)  
516 for advice and help, and particularly X. Pinson for critical reading of the manuscript. MRic is  
517 member of the national infrastructure France-BioImaging supported by the French National  
518 Research Agency (ANR-10-INBS-04). This work was supported by the *Centre National de la*  
519 *Recherche Scientifique (CNRS)*, the *Ligue Contre le Cancer Comités d'Ille et Vilaine, des Côtes*  
520 *d'Armor et du Finistère*, and the *Association pour la Recherche Contre le Cancer (ARC)* to G.B.

#### 521 522 **DISCLOSURES:**

523  
524 G.B. performed the experiments, wrote and reviewed the manuscript, and provided funding,  
525 M.T. reviewed the manuscript and provided support. M.T. is a scientific advisor and shareholder  
526 of the Inscoper company (France), which produces the solutions for rapid FLIM measurements  
527 shown in this manuscript. Inscoper partially supported the Open Access publication of the  
528 manuscript. Inscoper was not involved in experimental design, data handling, nor in the writing  
529 of the manuscript.

530

531 REFERENCES:

532

533 1. Bertolin, G., Tramier, M. Insights into the non-mitotic functions of Aurora kinase A: more  
534 than just cell division. *Cellular and Molecular Life Sciences*. doi: 10.1007/s00018-019-03310-2  
535 (2019).

536 2. Nikonova, A.S., Astsaturov, I., Serebriiskii, I.G., Dunbrack, R.L., Golemis, E.A. Aurora A  
537 kinase (AURKA) in normal and pathological cell division. *Cellular and Molecular Life Sciences*. **70**  
538 (4), 661–687, doi: 10.1007/s00018-012-1073-7 (2013).

539 3. Walter, A.O., Seghezzi, W., Korver, W., Sheung, J., Lees, E. The mitotic serine/threonine  
540 kinase Aurora2/AIK is regulated by phosphorylation and degradation. *Oncogene*. **19** (42), 4906–  
541 4916, doi: 10.1038/sj.onc.1203847 (2000).

542 4. Cheetham, G.M.T. Crystal Structure of Aurora-2, an Oncogenic Serine/Threonine Kinase.  
543 *Journal of Biological Chemistry*. **277** (45), 42419–42422, doi: 10.1074/jbc.C200426200 (2002).

544 5. Bayliss, R., Sardon, T., Vernos, I., Conti, E. Structural basis of Aurora-A activation by TPX2  
545 at the mitotic spindle. *Molecular cell*. **12** (4), 851–862 (2003).

546 6. Zhang, Y., Ni, J., Huang, Q., Ren, W., Yu, L., Zhao, S. Identification of the auto-inhibitory  
547 domains of Aurora-A kinase. *Biochemical and Biophysical Research Communications*. **357** (2),  
548 347–352, doi: 10.1016/j.bbrc.2007.03.129 (2007).

549 7. Littlepage, L.E., Wu, H., Andresson, T., Deanehan, J.K., Amundadottir, L.T., Ruderman, J.V.  
550 Identification of phosphorylated residues that affect the activity of the mitotic kinase Aurora-A.  
551 *Proceedings of the National Academy of Sciences of the United States of America*. **99** (24), 15440–  
552 15445, doi: 10.1073/pnas.202606599 (2002).

553 8. Kufer, T.A., Silljé, H.H.W., Körner, R., Gruss, O.J., Meraldi, P., Nigg, E.A. Human TPX2 is  
554 required for targeting Aurora-A kinase to the spindle. *The Journal of Cell Biology*. **158** (4), 617–  
555 623, doi: 10.1083/jcb.200204155 (2002).

556 9. Eyers, P.A., Erikson, E., Chen, L.G., Maller, J.L. A novel mechanism for activation of the  
557 protein kinase Aurora A. *Current Biology*. **13** (8), 691–697 (2003).

558 10. Brunet, S. *et al.* Characterization of the TPX2 Domains Involved in Microtubule Nucleation  
559 and Spindle Assembly in *Xenopus* Egg Extracts. *Molecular Biology of the Cell*. **15** (12), 5318–5328,  
560 doi: 10.1091/mbc.E04-05-0385 (2004).

561 11. Padilla-Parra, S., Tramier, M. FRET microscopy in the living cell: Different approaches,  
562 strengths and weaknesses. *BioEssays*. **34** (5), 369–376, doi: 10.1002/bies.201100086 (2012).

563 12. Aoki, K., Kamioka, Y., Matsuda, M. Fluorescence resonance energy transfer imaging of cell  
564 signaling from *in vitro* to *in vivo*: Basis of biosensor construction, live imaging, and image  
565 processing. *Development, Growth & Differentiation*. **55** (4), 515–522, doi: 10.1111/dgd.12039  
566 (2013).

567 13. Fuller, B.G. *et al.* Midzone activation of aurora B in anaphase produces an intracellular  
568 phosphorylation gradient. *Nature*. **453** (7198), 1132–1136, doi: 10.1038/nature06923 (2008).

569 14. Bertolin, G., Sizaire, F., Herbomel, G., Rebutier, D., Prigent, C., Tramier, M. A FRET  
570 biosensor reveals spatiotemporal activation and functions of aurora kinase A in living cells.  
571 *Nature Communications*. **7**, 12674, doi: 10.1038/ncomms12674 (2016).

572 15. Bertolin, G. *et al.* Optimized FRET Pairs and Quantification Approaches To Detect the  
573 Activation of Aurora Kinase A at Mitosis. *ACS Sensors*. **4** (8), 2018–2027, doi:  
574 10.1021/acssensors.9b00486 (2019).

- 575 16. Bertolin, G. *et al.* Aurora kinase A localises to mitochondria to control organelle dynamics  
576 and energy production. *eLife*. **7**, doi: 10.7554/eLife.38111 (2018).
- 577 17. Sizaire, F., Le Marchand, G., Pécréaux, J., Bouchareb, O., Tramier, M. Automated  
578 screening of AURKA activity based on a genetically encoded FRET biosensor using fluorescence  
579 lifetime imaging microscopy. *Methods and Applications in Fluorescence*. **8** (2), 024006, doi:  
580 10.1088/2050-6120/ab73f5 (2020).
- 581 18. Demeautis, C. *et al.* Multiplexing PKA and ERK1&2 kinases FRET biosensors in living  
582 cells using single excitation wavelength dual colour FLIM. *Scientific Reports*. **7**, 41026, doi:  
583 10.1038/srep41026 (2017).
- 584 19. Ringer, P. *et al.* Multiplexing molecular tension sensors reveals piconewton force gradient  
585 across talin-1. *Nature Methods*. **14** (11), 1090–1096, doi: 10.1038/nmeth.4431 (2017).
- 586 20. Nagai, T., Yamada, S., Tominaga, T., Ichikawa, M., Miyawaki, A. Expanded dynamic range  
587 of fluorescent indicators for Ca(2+) by circularly permuted yellow fluorescent proteins.  
588 *Proceedings of the National Academy of Sciences of the United States of America*. **101** (29),  
589 10554–10559, doi: 10.1073/pnas.0400417101 (2004).
- 590 21. Klarenbeek, J., Goedhart, J., Batenburg, A. van, Groenewald, D., Jalink, K. Fourth-  
591 Generation Epac-Based FRET Sensors for cAMP Feature Exceptional Brightness, Photostability  
592 and Dynamic Range: Characterization of Dedicated Sensors for FLIM, for Ratiometry and with  
593 High Affinity. *PLOS ONE*. **10** (4), e0122513, doi: 10.1371/journal.pone.0122513 (2015).
- 594 22. Fritz, R.D. *et al.* A Versatile Toolkit to Produce Sensitive FRET Biosensors to Visualize  
595 Signaling in Time and Space. *Science Signaling*. **6** (285), rs12–rs12, doi: 10.1126/scisignal.2004135  
596 (2013).
- 597 23. Mastop, M., Bindels, D.S., Shaner, N.C., Postma, M., Gadella, T.W.J., Goedhart, J.  
598 Characterization of a spectrally diverse set of fluorescent proteins as FRET acceptors for  
599 mTurquoise2. *Scientific Reports*. **7** (1), 11999, doi: 10.1038/s41598-017-12212-x (2017).
- 600 24. van der Krogt, G.N.M., Ogink, J., Ponsioen, B., Jalink, K. A Comparison of Donor-Acceptor  
601 Pairs for Genetically Encoded FRET Sensors: Application to the Epac cAMP Sensor as an Example.  
602 *PLoS ONE*. **3** (4), e1916, doi: 10.1371/journal.pone.0001916 (2008).
- 603 25. Cranfill, P.J. *et al.* Quantitative assessment of fluorescent proteins. *Nature Methods*. **13**  
604 (7), 557–562, doi: 10.1038/nmeth.3891 (2016).
- 605 26. Goedhart, J. *et al.* Structure-guided evolution of cyan fluorescent proteins towards a  
606 quantum yield of 93%. *Nature Communications*. **3** (1), doi: 10.1038/ncomms1738 (2012).
- 607 27. Mérola, F., Fredj, A., Betolngar, D.-B., Ziegler, C., Erard, M., Pasquier, H. Newly engineered  
608 cyan fluorescent proteins with enhanced performances for live cell FRET imaging. *Biotechnology*  
609 *Journal*. **9** (2), 180–191, doi: 10.1002/biot.201300198 (2014).
- 610 28. Erard, M. *et al.* Minimum set of mutations needed to optimize cyan fluorescent proteins  
611 for live cell imaging. *Molecular BioSystems*. **9** (2), 258–267, doi: 10.1039/C2MB25303H (2013).
- 612 29. Tramier, M., Zahid, M., Mevel, J.-C., Masse, M.-J., Coppey-Moisan, M. Sensitivity of  
613 CFP/YFP and GFP/mCherry pairs to donor photobleaching on FRET determination by fluorescence  
614 lifetime imaging microscopy in living cells. *Microscopy Research and Technique*. **69** (11), 933–939,  
615 doi: 10.1002/jemt.20370 (2006).
- 616 30. Padilla-Parra, S., Audugé, N., Lalucque, H., Mevel, J.-C., Coppey-Moisan, M., Tramier, M.  
617 Quantitative Comparison of Different Fluorescent Protein Couples for Fast FRET-FLIM  
618 Acquisition. *Biophysical Journal*. **97** (8), 2368–2376, doi: 10.1016/j.bpj.2009.07.044 (2009).

- 619 31. Burgstaller, S. *et al.* pH-Lemon, a Fluorescent Protein-Based pH Reporter for Acidic  
620 Compartments. *ACS Sensors*. doi: 10.1021/acssensors.8b01599 (2019).
- 621 32. Bindels, D.S. *et al.* mScarlet: a bright monomeric red fluorescent protein for cellular  
622 imaging. *Nature Methods*. **14** (1), 53–56, doi: 10.1038/nmeth.4074 (2016).
- 623 33. Murakoshi, H., Shibata, A.C.E., Nakahata, Y., Nabekura, J. A dark green fluorescent protein  
624 as an acceptor for measurement of Förster resonance energy transfer. *Scientific Reports*. **5**,  
625 15334, doi: 10.1038/srep15334 (2015).
- 626 34. Murakoshi, H., Shibata, A.C.E. ShadowY: a dark yellow fluorescent protein for FLIM-based  
627 FRET measurement. *Scientific Reports*. **7** (1), 6791, doi: 10.1038/s41598-017-07002-4 (2017).
- 628 35. Leray, A., Padilla-Parra, S., Roul, J., Héliot, L., Tramier, M. Spatio-Temporal Quantification  
629 of FRET in living cells by fast time-domain FLIM: a comparative study of non-fitting methods  
630 [corrected]. *PloS One*. **8** (7), e69335, doi: 10.1371/journal.pone.0069335 (2013).
- 631 36. Padilla-Parra, S., Audugé, N., Coppey-Moisan, M., Tramier, M. Quantitative FRET analysis  
632 by fast acquisition time domain FLIM at high spatial resolution in living cells. *Biophysical Journal*.  
633 **95** (6), 2976–2988, doi: 10.1529/biophysj.108.131276 (2008).
- 634 37. Song, L., Hennink, E.J., Young, I.T., Tanke, H.J. Photobleaching kinetics of fluorescein in  
635 quantitative fluorescence microscopy. *Biophysical Journal*. **68** (6), 2588–2600, doi:  
636 10.1016/S0006-3495(95)80442-X (1995).
- 637 38. Manfredi, M.G. *et al.* Characterization of Alisertib (MLN8237), an investigational small-  
638 molecule inhibitor of aurora A kinase using novel in vivo pharmacodynamic assays. *Clinical Cancer*  
639 *Research: An Official Journal of the American Association for Cancer Research*. **17** (24), 7614–  
640 7624, doi: 10.1158/1078-0432.CCR-11-1536 (2011).
- 641 39. Katayama, H. *et al.* Phosphorylation by aurora kinase A induces Mdm2-mediated  
642 destabilization and inhibition of p53. *Nature Genetics*. **36** (1), 55–62, doi: 10.1038/ng1279 (2004).
- 643 40. Nowakowski, J. *et al.* Structures of the Cancer-Related Aurora-A, FAK, and EphA2 Protein  
644 Kinases from Nanovolume Crystallography. *Structure*. **10** (12), 1659–1667, doi: 10.1016/S0969-  
645 2126(02)00907-3 (2002).
- 646 41. Palmer, A.E., Qin, Y., Park, J.G., McCombs, J.E. Design and application of genetically  
647 encoded biosensors. *Trends in Biotechnology*. **29** (3), 144–152, doi:  
648 10.1016/j.tibtech.2010.12.004 (2011).
- 649 42. Grant, R. *et al.* Constitutive regulation of mitochondrial morphology by Aurora A kinase  
650 depends on a predicted cryptic targeting sequence at the N-terminus. *Open Biology*. **8** (6),  
651 170272, doi: 10.1098/rsob.170272 (2018).
- 652 43. Shimosono, S., Miyawaki, A. Engineering FRET Constructs Using CFP and YFP. *Methods in*  
653 *Cell Biology*. **85**, 381–393, doi: 10.1016/S0091-679X(08)85016-9 (2008).
- 654 44. Komatsu, N. *et al.* Development of an optimized backbone of FRET biosensors for kinases  
655 and GTPases. *Molecular Biology of the Cell*. **22** (23), 4647–4656, doi: 10.1091/mbc.e11-01-0072  
656 (2011).
- 657 45. Schifferer, M., Griesbeck, O. A Dynamic FRET Reporter of Gene Expression Improved by  
658 Functional Screening. *Journal of the American Chemical Society*. **134** (37), 15185–15188, doi:  
659 10.1021/ja3055673 (2012).
- 660 46. Peroza, E.A., Boumezbeur, A.-H., Zamboni, N. Rapid, randomized development of  
661 genetically encoded FRET sensors for small molecules. *Analyst*. **140** (13), 4540–4548, doi:  
662 10.1039/C5AN00707K (2015).

- 663 47. Rebutier, D. *et al.* Aurora A is involved in central spindle assembly through  
664 phosphorylation of Ser 19 in P150Glued. *The Journal of cell biology*. **201** (1), 65–79 (2013).
- 665 48. Mo, G.C.H., Posner, C., Rodriguez, E.A., Sun, T., Zhang, J. A rationally enhanced red  
666 fluorescent protein expands the utility of FRET biosensors. *Nature Communications*. **11** (1), 1848,  
667 doi: 10.1038/s41467-020-15687-x (2020).
- 668